NeuroImage: Clinical 11 (2016) 694–706

Contents lists available at ScienceDirect

NeuroImage: Clinical

journal homepage: www.elsevier.com/locate/ynicl

DTI-based response-driven modeling of mTLE laterality☆

Mohammad-Reza Nazem-Zadeh[a,*], Kost Elisevich[b], Ellen L. Air[c], Jason M. Schwalb[c], George Divine[d], Manpreet Kaur[c], Vibhangini S. Wasade[e], Fariborz Mahmoudi[a,f], Saeed Shokri[a,g], Hassan Bagher-Ebadian[a,e], Hamid Soltanian-Zadeh[a,h]

[a] Radiology and Research Administration Department, Henry Ford Health System, Detroit, MI 48202, USA
[b] Department of Clinical Neurosciences, Spectrum Health Medical Group, Division of Neurosurgery, Michigan State University, Grand Rapids, MI 49503, USA
[c] Neurosurgery Department, Henry Ford Health System, Detroit, MI 48202, USA
[d] Public Health Sciences Department, Henry Ford Health System, Detroit, MI 48202, USA
[e] Neurology Department, Henry Ford Health System, Detroit, MI 48202, USA
[f] Computer and IT engineering Faculty, Islamic Azad University, Qazvin Branch, Iran
[g] School of Computer Science, Wayne State University, Detroit, MI 48202, USA
[h] Control and Intelligent Processing Center of Excellence (CIPCE), School of Electrical and Computer, University of Tehran, Tehran, Iran

ARTICLE INFO

Article history:
Received 1 June 2015
Received in revised form 25 October 2015
Accepted 27 October 2015
Available online 30 October 2015

Keywords:
Response-driven lateralization models
Diffusion tensor imaging
Bilateral
Bitemporal
Mesial temporal lobe epilepsy

ABSTRACT

Purpose: To develop lateralization models for distinguishing between unilateral and bilateral mesial temporal lobe epilepsy (mTLE) and determining laterality in cases of unilateral mTLE.
Background: mTLE is the most common form of medically refractory focal epilepsy. Many mTLE patients fail to demonstrate an unambiguous unilateral ictal onset. Intracranial EEG (icEEG) monitoring can be performed to establish whether the ictal origin is unilateral or truly bilateral with independent bitemporal ictal origin. However, because of the expense and risk of intracranial electrode placement, much research has been done to determine if the need for icEEG can be obviated with noninvasive neuroimaging methods, such as diffusion tensor imaging (DTI).
Methods: Fractional anisotropy (FA) was used to quantify microstructural changes reflected in the diffusivity properties of the corpus callosum, cingulum, and fornix, in a retrospective cohort of 31 patients confirmed to have unilateral (n = 24) or bilateral (n = 7) mTLE. All unilateral mTLE patients underwent resection with an Engel class I outcome. Eleven were reported to have hippocampal sclerosis on pathological analysis; nine had undergone prior icEEG. The bilateral mTLE patients had undergone icEEG demonstrating independent epileptiform activity in both right and left hemispheres. Twenty-three nonepileptic subjects were included as controls.
Results: In cases of right mTLE, FA showed significant differences from control in all callosal subregions, in both left and right superior cingulate subregions, and in forniceal crura. Comparison of right and left mTLE cases showed significant differences in FA of callosal genu, rostral body, and splenium and the right posteroinferior and superior cingulate subregions. In cases of left mTLE, FA showed significant differences from control only in the callosal isthmus. Significant differences in FA were identified when cases of right mTLE were compared with bilateral mTLE cases in the rostral and midbody callosal subregions and isthmus. Based on 11 FA measurements in the cingulate, callosal and forniceal subregions, a response-driven lateralization model successfully differentiated all cases (n = 54) into groups of unilateral right (n = 12), unilateral left (n = 12), and bilateral mTLE (n = 7), and nonepileptic control (23).
Conclusion: The proposed response-driven DTI biomarker is intended to lessen diagnostic ambiguity of laterality in cases of mTLE and help optimize selection of surgical candidates. Application of this model shows promise in reducing the need for invasive icEEG in prospective cases.

☆ This work was supported in part by NIH grant R01-EB013227.
* Corresponding author at: Radiology and Administration Departments, Henry Ford Health System, Detroit, MI 48202, USA.
E-mail addresses: kost.elisevich@spectrumhealth.org, mnazemz1@hfhs.org (M.-R. Nazem-Zadeh), eair1@hfhs.org (E.L. Air), jschwal1@hfhs.org (J.M. Schwalb), gdivine1@hfhs.org (G. Divine), mkaur1@hfhs.org (M. Kaur), vwasade1@hfhs.org (V.S. Wasade), fmahmou1@hfhs.org (F. Mahmoudi), sshokri1@hfhs.org (S. Shokri), hbagher1@hfhs.org (H. Bagher-Ebadian), hsoltan1@hfhs.org, hszadeh@ut.ac.ir (H. Soltanian-Zadeh).

http://dx.doi.org/10.1016/j.nicl.2015.10.015

1. Introduction

1.1. Temporal lobe epilepsy and intracranial EEG

According to the World Health Organization, more than fifty million people worldwide and three million people in the USA suffer from epilepsy — a disorder characterized by recurrent, spontaneous seizures (Hirtz et al., 2007). Mesial temporal lobe epilepsy (mTLE) is the most common form of surgically remediable focal epilepsy, accounting for 60–75% of patients undergoing surgery for medically refractory epilepsy (Engel, 1996). Many mTLE patients with truly unilateral epileptogenicity cannot be clearly defined as such using noninvasive measures such as scalp EEG, structural magnetic resonance imaging (MRI), seizure semiology, and neuropsychology (Dupont et al., 2015; Javidan, 2012; Mansouri et al., 2012; Sperling et al., 1992). Scalp EEG may suggest a bilateral mTLE when, in fact, the condition is unilateral. In a recent study, 1026 (73%) out of 1403 patients presumed to have bilateral mTLE on scalp EEG were found to have a unilateral mTLE by intracranial EEG (icEEG) (Aghakhani et al., 2014). Conversely, about 10–20% of all mTLE patients have true bilateral mTLE, with ictal onsets arising independently in both hemispheres (Hirsch et al., 1991; Hufnagel et al., 1994; Kuba et al., 2003; Řehulka et al., 2014; So et al., 1989). Such patients are not candidates for surgical resection. Although on the basis of scalp EEG and seizure semiology, some cases may be correctly determined to be unilateral (Marks and Laxer, 1998; Serles et al., 2000) or bilateral (Loesch et al., 2014; Řehulka et al., 2014), icEEG monitoring remains the gold standard for defining unilateral versus bilateral epileptogenicity (Bulacio et al., 2012; Pacia and Ebersole, 1999; Sperling et al., 1992).

1.2. Disadvantages of icEEG

Intracranial electrode implantation for extraoperative electrocorticography delays definitive surgical treatment, increases the expense of investigation (Bulacio et al., 2012; Kuzniecky et al., 1997), and carries significant risks of infection, intracranial hemorrhage and elevated intracranial pressure (Arya et al., 2013). This has spurred many groups, including ours, to investigate whether noninvasive neuroimaging methods (Aghakhani et al., 2014; Zhang et al., 2014) can detect the microstructural changes that are associated with different seizure activities, thereby obviating the need for icEEG.

1.3. Neuroimaging for detection of structural change

The chronic effects of epileptogenesis lead to progressive structural changes that may be detected using neuroimaging modalities such as structural MRI, MR spectroscopy, and diffusion tensor imaging (DTI). Hippocampal atrophy on T1-weighted imaging and hyperintensity on Fluid Attenuated Inversion Recovery (FLAIR) imaging in the hippocampus, amygdala, or temporal neocortex, ipsilateral to the side of seizure onset, often typifies the appearance of pathology, known as mesial temporal sclerosis (MTS) (Aroniadou-Anderjaska et al., 2008; Jafari-Khouzani et al., 2006, 2010; Pereira et al., 2005). Although MTS remains a useful predictor of successful surgery for epilepsy (Achten et al., 1997; de Tisi et al., 2011; Engel, 1996; Vainio et al., 1994), there have been reports of patients with pathologically-confirmed hippocampal sclerosis without abnormalities on T1-weighted and FLAIR imaging (Yang et al., 2014). Moreover, structural MRI may not detect subtle chronic epileptogenic alterations in non-MTS mTLE types.

1.4. DTI as an early biomarker of microstructural changes

DTI is an MRI technique that measures the overall magnitude (i.e., diffusivity) and directionality (i.e., anisotropy) of molecular displacement (Pierpaoli et al., 2001) due to Brownian motion (Le Bihan et al., 1986). It can detect microstructural changes in brain tissue before any abnormality appears on structural MRI (Eriksson et al., 2001; Hufnagel et al., 2003; Nakasu et al., 1995; Parekh et al., 2010; Rugg-Gunn et al., 2001; Szabo et al., 2005; Wall et al., 2000). Neuronal loss at the seizure focus in mTLE results in alteration of white matter tracts connecting the focus to other brain regions, which then may cause structural changes in remote but anatomically connected brain regions (Scanlon et al., 2013). Since propagation of synchronized neuronal firing in mTLE is widespread, extralimbic structures can also be affected (Aroniadou-Anderjaska et al., 2008; Bernasconi et al., 1999, 2003; Chahboune et al., 2009; Concha et al., 2004, 2005, 2009; de Curtis and Paré, 2004; Gross et al., 2006; Kim et al., 2008, 2010; Kuo et al., 2008; Laitinen et al., 2010; Liacu et al., 2012b; Liu et al., 2012; Parekh et al., 2010; Pereira et al., 2005; Thivard et al., 2005). Thus, DTI holds potential as a useful tool for investigating deficits in the integrity of temporal and extratemporal white matter fiber tracts involved in mTLE (Liu et al., 2014; Mishra et al., 2011; Rugg-Gunn et al., 2001; Waites et al., 2006; Wall et al., 2000; Yogarajah and Duncan, 2008). Diminished local structural connectivity of cortical regions throughout the default mode network (DMN) has been seen in patients with mTLE compared to healthy subjects (Chiang and Haneef, 2014; DeSalvo et al., 2014; Vaessen et al., 2011). An analogous decrease in functional connectivity has been noted using functional MRI (fMRI) (Pittau et al., 2012; Skudlarski et al., 2008). Also, a widespread increase in global network efficiency has been seen within the DMN in mTLE patients (Chiang and Haneef, 2014; DeSalvo et al., 2014; Vaessen et al., 2011) relative to nonepileptic controls, implying that epileptogenicity promotes signal propagation along certain pathways.

1.5. Gray matter changes attributed to mTLE

MRI studies in cases of mTLE have documented abnormalities in limbic and extralimbic structures of the hippocampus throughout its four main histological divisions (CA1–4) (Bernasconi et al., 2003), the parahippocampal gyrus (Bernasconi et al., 2003), entorhinal cortex (Bernasconi et al., 1999, 2003), piriform cortex (Pereira et al., 2005), amygdala (Aroniadou-Anderjaska et al., 2008; de Curtis and Paré, 2004; Pereira et al., 2005), and thalamus (Parekh et al., 2010) in mTLE. Excitotoxic neuronal injury at sites of focal epileptogenicity may lead to a loss of volume and alteration in diffusion properties in such structures, including a global alteration relative to nonepileptic cases, or interhemispheric asymmetry in each case (Nazem-Zadeh et al., 2014b).

1.6. White matter changes attributed to mTLE

Abnormalities have also been documented in the white matter structures of cingulum (Concha et al., 2004, 2009), fornix (Concha et al., 2004), corpus callosum (Chahboune et al., 2009), uncinate fasciculus (Rodrigo et al., 2007), external capsule (Gross et al., 2006), arcuate fasciculus (Powell et al., 2007), hippocampal mossy fibers (Kuo et al., 2008; Laitinen et al., 2010), and thalamic fibers (Bonilha et al., 2012). The cingulum and fornix are integral components of the limbic circuit that mediate the expression of epileptogenicity arising from mesial temporal structures (Ahmadi et al., 2009; Concha et al., 2004, 2009, 2010; Liacu et al., 2012b; Yoo et al., 2002). The TLE-induced alteration makes them suitable candidates as biomarkers of laterality. Interhemispheric variation of FA in the posteroinferior cingulum and crus of the fornix have lateralized mTLE in individual cases (Nazem-Zadeh et al., 2014b). The corpus callosum connects the inferior temporal and occipital regions as well as superior temporal and parietal regions of each hemisphere at its isthmus and splenium, respectively (Firat et al., 2014; Weber et al., 2007). These subregions have, likewise, been found to be affected by mTLE (Firat et al., 2014; Hermann et al., 2003; Weber et al., 2007).

1.7. DTI findings with structural changes

The related microstructural changes can be detected using segmentation or fiber tracking (FT) with DTI data. Most previous studies have reported bilateral alterations of fractional anisotropy (FA) and mean diffusivity (MD), as indices of fiber integrity and overall diffusivity, respectively (Nazem-Zadeh et al., 2012a; Pierpaoli et al., 2001) as a way to differentiate the DTI-based structural changes in subjects with unilateral mTLE from those in nonepileptic controls (Concha et al., 2004, 2009, 2010; Gross et al., 2006; Hugg et al., 1999; Kim et al., 2008, 2010; Liacu et al., 2012b; Rugg-Gunn et al., 2001; Thivard et al., 2005; Wieshmann et al., 1999; Yogarajah and Duncan, 2008). Some have reported upon the capability of DTI to lateralize mTLE by comparing variations among patients with mTLE and nonepileptic subjects (Ahmadi et al., 2009; Focke et al., 2008; Nazem-Zadeh et al., 2014b; Yoo et al., 2002), but most have not applied DTI to lateralize epileptogenicity in individual mTLE patients, and none have reported its capability to differentiate bilateral from unilateral cases.

We hypothesized that a multistructural analysis of DTI changes in the cingulum, fornix and corpus callosum can differentiate between subjects with and without epilepsy and can serve as effective quantitative neuroimaging biomarkers to distinguish between unilateral and bilateral mTLE, as well as to specify laterality. This represents a novel approach to the noninvasive lateralization of mTLE.

2. Materials and methods

2.1. Human subjects

This research study was approved by the Henry Ford Health System Institutional Review Board and involved 31 patients with mTLE. Seven patients had bilateral mTLE confirmed by icEEG (male:female, 3:4; ages 33.1 ± 12.5 years and 38.3 ± 7.5 years, respectively). Twenty-four patients had unilateral mTLE, achieving an Engel class I outcome following resection of their mesial temporal structure (male:female, 13:11; ages 41.8 ± 12.9 years and 42.0 ± 12.8 years, respectively), 9 of whom had undergone prior icEEG and 11 were reported to have hippocampal sclerosis on pathological analysis (Table 1). A cohort of 23 nonepileptic subjects (male:female, 15:8; ages 30.6 ± 3.6 years and 34.6 ± 7.9 years, respectively) served as controls to establish a boundary (i.e., control) domain and account for any natural variance in the proposed model. The side of epileptogenicity was blinded during all processing.

2.2. Image acquisition

All subjects underwent preoperative imaging in a single 3.0 T MRI system using a standardized protocol for image acquisition. T1-weighted images were acquired using the spoiled gradient echo protocol (SPGR) with TR/TI/TE = 10,400/4500/300 ms, flip angle = 15°, voxel size = $0.39 \times 0.39 \times 2.00$ mm^3. FLAIR images were also acquired with TR/TI/TE = 9002/2250/124 ms, flip angle = 90°, voxel size = $0.39 \times 0.39 \times 3.00$ mm^3. DTI images (b-value of 1000 s/mm^2) in 25 diffusion gradient directions along with a set of null images (b-value of 0 s/mm^2) were acquired using echo planar imaging (EPI) with TR/TI/TE = 10,000/0/76 ms, flip angle = 90°, voxel size = $1.96 \times 1.96 \times 2.6$ mm^3

2.3. Image pre-processing

Before segmenting the white matter structures of interest, the DTI images were prepared by interpolation to a homogeneous voxel size of 1.96 mm isotropic resolution with subsequent tensor, FA and MD calculation (Nazem-Zadeh et al., 2012a; Pierpaoli et al., 2001). For the purpose of segmentation, the principal diffusion direction (PDD), the eigenvector corresponding to the largest eigenvalue of the tensor, was also calculated from the tensor.

2.4. Segmentation of the cingulum, fornix, corpus callosum and their subregions

The cingulum and its subregions were established using an automatic seed-based segmentation and fiber tracking algorithm (Nazem-Zadeh et al., 2012a), and included: 1 — insertion of seed points on both left and right sides of the cingulum in sagittal views; 2 — automatic extraction of a two-dimensional region of interest (ROI) for each seed point; 3 — fiber tracking between consecutive ROIs; 4 — postprocessing of the segmented structure through a morphological operation consisting of a dilation followed by an erosion using a cubical structuring element with $2 \times 3 \times 3$ voxels (Nazem-Zadeh et al., 2012a); and 5 — division of each segmented left and right cingulum into three subregions (i.e., posteroinferior, superior, and anteroinferior) using the points with highest curvature on the mesial axis.

The corpus callosum and its subregions were established using an automatic seed-based segmentation algorithm, and included: 1 — automatic three-dimensional segmentation using a level-set algorithm based on tensor similarities between neighboring voxels of a growing surface boundary (Nazem-Zadeh et al., 2012b); and 2 — extraction of the main axes using principal component analysis (PCA) and division into Witelson subregions of genu (including rostrum), rostral body, anterior midbody, posterior midbody, isthmus and splenium (Nazem-Zadeh et al., 2013; Witelson, 1989).

The fornix was also established using a multiple ROI fiber-tracking algorithm (Nazem-Zadeh et al., 2012a), and included: 1 — manual depiction of three coronal ROIs at the most anterior part of the forniceal body, the branching point of the forniceal body from the crura and between the branching point and the most posterior part of the forniceal crura; 2 — manual depiction of two axial ROIs at the most posterior and the most inferior parts of the forniceal crura; 3 — fiber-tracking between consecutive ROIs; and 4 — division of the fornix into three subregions of anterior body, left crus and right crus using the branching point of the forniceal crura from the body (Fig 1).

2.5. Hippocampal T_1 volumetry and FLAIR intensity analysis

The volumes of both left and right hippocampi from 31 mTLE patients and 23 nonepileptic subjects were established from the ROIs drawn manually using standard protocol of hippocampal delineation (Jafari-Khouzani et al., 2011). The hippocampal head, body and tail were outlined. While the subiculum was also included, the amygdala and temporal horn of the lateral ventricle, and white matter tracts, including the alveus and fimbria, were not included. The alveus was used as a landmark separating the amygdala and hippocampus. The most anterior coronal slice was taken where the alveus demarcated the hippocampal head as it tapered below the amygdala. The hippocampal tail was taken to a posterior point where it narrowed and curved medially towards the crus. The gray-white matter interface was used as the inferior and lateral border (Jafari-Khouzani et al., 2011). Using an affine registration tool (FLIRT; (Jenkinson et al., 2002)) and T_1 images, the hippocampal boundaries were coregistered to FLAIR images to acquire the mean and standard deviation of FLAIR intensity within the hippocampus (Akhondi-Asl et al., 2011; Jafari-Khouzani et al., 2010).

2.6. Structural change analysis

T-tests and one-way analysis of variance were used to compare mean ages for patients and controls, and among the three locations (unilateral mTLE, bilateral mTLE, and control), respectively. A chi-square test was used to compare gender proportions. Two-way repeated measures analysis of variance (RMANOVA) was used to examine the relationships between FA measurements and hippocampal measurements (i.e., the volumes on T1-weighted images and means and standard deviations of signal intensities on FLAIR images) with the brain

Table 1
The patient characteristics, neuroclinical findings and neuroimaging lateralization results.

Patient number	Age at the surgery[a]	Gender	Lateralization by EEG Phase I	Lateralization by WADA test	Lateralization by neuropsychological tests	icEEG	icEEG strategy	Side of epileptogenicity[b]	Pathology-proven MTS	Lateralization by FA in posteroinferior cingulum	Lateralization by FA in fornix	Lateralization by hippocampal volume	Lateralization by hippocampal FLAIR intensity	Lateralization by the proposed model M3
1	30	M	L Tmp	L	L	N	–	L	NA	L	L	L	L	L
2	31	M	R Tmp	N	R	Y	R Frt-Tmp	R	N	N	R	R	L	R
3	30	M	L Tmp	L	N	Y	L Tmp	L	Y	N	L	N	L	L
4	46	M	bi-Tmp L > R	L	L	Y	bi-Tmp	L	Y	L	L	L	L	L
5	28	M	R Tmp	R	R	N	–	R	NA	N	R	R	R	R
6	44	M	bi-Tmp, R > L, R and L Frt	R	N	Y	bi-Tmp	R	NA	L	R	N	L	R
7	40	F	L Tmp	N	L	N	–	L	NA	L	N	L	N	L
8	29	M	L Tmp	R	N	N	–	L	NA	L	N	L	L	L
9	44	F	L Tmp	L	L	N	–	L	Y	L	L	L	L	L
10	53	M	L Tmp, convexity focus	L	L	Y	L Tmp	L	Y	L	L	L	L	L
11	65	F	Bi-Tmp	N	N	N	icEEG during surgery	R	N	N	N	N	L	R
12	48	F	R Tmp	R	R	N	–	R	NA	N	R	R	R	R
13	61	M	L Tmp	L	N	N	–	L	Y	L	L	L	L	L
14	38	F	L Tmp	L	N	N	icEEG during surgery	L	N	N	N	L	N	L
15	29	F	R Tmp	R	R	N	–	R	NA	N	R	R	L	R
16	61	M	L Tmp	L	R	N	–	L	Y	L	L	L	L	L
17	28	M	R Tmp	R	N	N	–	R	NA	N	N	N	R	R
18	48	F	R Tmp, R Ins	R	R	Y	R Tmp + R Ins	R	Y	R	R	R	R	R
19	52	F	L Tmp	N	L	N	–	L	Y	L	R	L	L	L
20	53	M	R Tmp, R Occ, R neocortex and R insula interictal	R	R	Y	bi-Tmp + R Frt	R	NA	N	N	L	N	R
21	15	F	R Tmp	N	L	Y	bi-Tmp	R	Y	R	R	R	R	R
22	49	M	R Tmp	R	R	N	–	R	Y	R	R	R	R	R
23	45	F	R Tmp neocortex, R Frt-Prt interictal	R	R	Y	R Tmp + R Prt	R	NA	R	L	N	R	R
24	38	F	L Tmp	L	L	N	–	L	Y	L	N	L	L	L
25	34	F	bi-Tmp R = L	N	R	Y	bi-Tmp	B	NA	L	N	N	N	B
26	35	M	L Tmp	N	NA	Y	bi-Tmp	B	NA	N	N	N	N	B
27	20	M	L Tmp, L-Frt-Tmp, R-Frt-Cnt, rare bi-Frt interictal	NA	NA	Y	bi-Tmp	B	NA	N	N	N	L	B
28	46	F	bi-Tmp R > L (R ictal and R and L interictal)											
Frt-Tmp-Cnt,	R	L	Y	bi-Tmp	B	NA	R	N	L	N	B			
29	43	F	bi-Tmp R > L	L	NA	Y	bi-Tmp	B	NA	N	N	N	R	B
30	30	F	bi-Tmp R = L	R	R	Y	bi-Tmp	B	NA	L	N	L	N	B
31	44	M	bi-Tmp R = L	N	NA	Y	bi-Tmp	B	NA	N	N	N	N	B

Table notes: Tmp: temporal, Occ: occipital, Frt: frontal, Prt: parietal, Ins: insular, Cnt: central, bi-Tmp: bitemporal, bi-Frt: bifrontal, L: left, R: right, B: bilateral mTLE. N: non-lateralizing, NA: not available.
Note that except for the proposed model M3, there were some mTLE cases for which the other lateralization methods including neuroclinical ones failed to detect the epileptogenic side, with either a false positive, or a nonlateralizing result.

[a] Age at icEEG only for bilateral mTLE cases.

[b] For the patients with icEEG, icEEG findings, and for the patient without icEEG, the multi-disciplinary decision made on the laterality prior to the surgery will serve as the source of truth for the side of epileptogenicity.

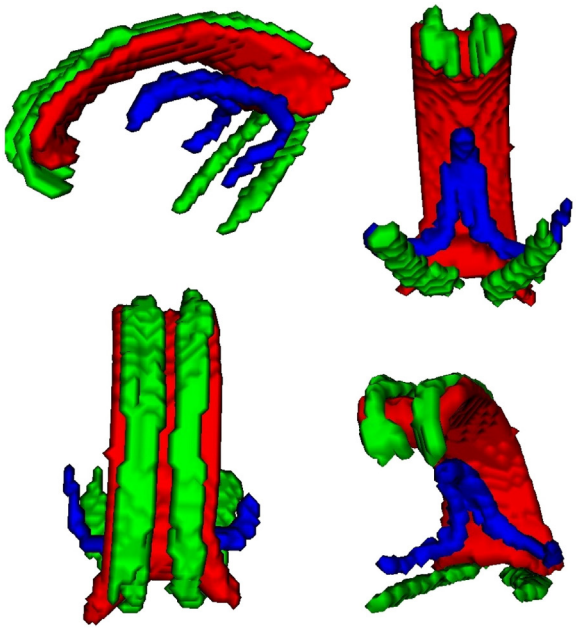

(a)

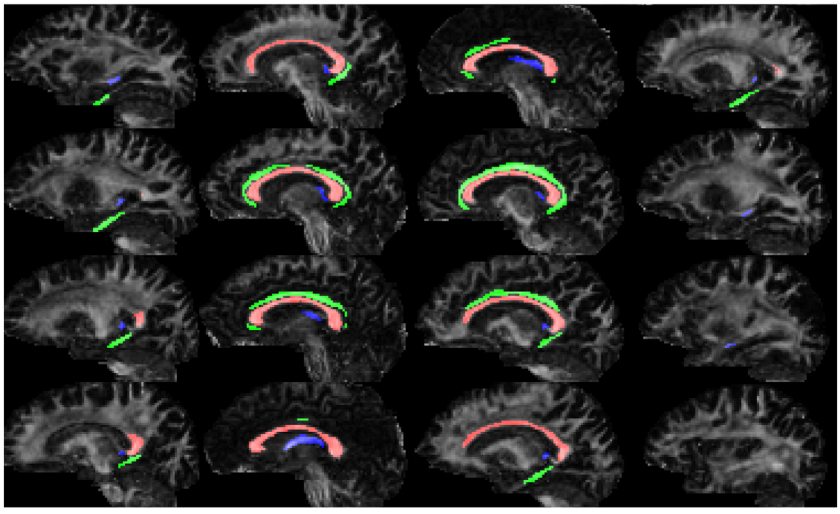

(b)

Fig. 1. The segmented corpus callosum (red), cingulum (green), and fornix (blue) (a): in three-dimensional views, (b): with overlaid segments on FA sagittal images.

region (i.e., a repeated factor) and mTLE laterality type (i.e., a fixed factor). Of particular interest were tests for interaction between region and laterality type, since significant interaction implies that separate one-way ANOVAs are required to assess mTLE laterality type effects by holding the region constant, and separate one-way RMANOVAs are required to assess region effects by holding mTLE laterality type constant. For each region, one-way ANOVA on mTLE laterality type was performed, but was considered statistically significant only if the overall ANOVA F-test for all mTLE laterality types was also significant after a multiple comparisons adjustment. For each mTLE laterality type, one-way RMANOVA was performed for the corpus callosum, cingulum, and fornix regions followed by paired t-tests between pairs of their subregions (i.e., adjacent subregions in corpus callosum, cingulum, and fornix and corresponding left and right subregions in cingulum and fornix). A paired t-test between subregions in a structure was considered statistically significant only if the overall RMANOVA F-test was also significant in the entire corresponding structure, and its p-value was below a level determined by a multiple comparisons adjustment. Multiple comparisons were addressed by separate Bonferroni adjustments for six pairwise comparisons between laterality types and 21 comparisons between regions (15 for FA measurements and 6 for hippocampal measurements including volumes, and FLAIR means and standard deviations) for the one-way ANOVAs; and for 18 pairwise comparisons between regions and six comparisons among mTLE groups for RMANOVAs.

2.7. Development of lateralization response-driven models

The FA or MD indices within the subregions of the cingulum (i.e., anteroinferior left and right, superior left and right, and posteroinferior left and right), the subregions of the corpus callosum (i.e., genu, rostral body, anterior midbody, posterior midbody, isthmus,

splenium) and the subregions of the fornix (i.e., anterior body, left and right crus) were extracted for cohorts of unilateral mTLE, bilateral mTLE, and control. These multivariate features were considered as independent variables and incorporated into the development of three response-driven models of the laterality using multinomial logistic function regression (Hosmer et al., 2013). The laterality label (i.e., L = unilateral left mTLE, R = unilateral right mTLE, U = unilateral mTLE, B = bilateral mTLE and N = non-lateralizing) was considered the dependent variable.

Model 1: Right mTLE vs. Left mTLE
Model 2: Unilateral mTLE vs. Bilateral mTLE
Model 3: Right mTLE vs. Left mTLE vs. Bilateral mTLE vs. Control

In order to assess how the multinomial logistic function generalized to an independent dataset and how accurately this response model performed in practice, a cross-validation was performed using the 'leave-one-out' approach for 54 repetitions considering a single case as validation data and the remaining 53 cases as training data (Picard and Cook, 1984). The multinomial logistic models were regressed to training data as follows:

$$\ln\left(\frac{\Pr(Y_i = T|M_k)}{\Pr(Y_i = N|M_k)}\right) = \beta_T^k \cdot X_i^k \quad (1)$$

where X_i^k is a vector of i^{th} observation in the training dataset incorporated in Model k, $\Pr(Y_i = T|M_k)$ and β_T^k are the posterior probability of the epileptogenic side Y_i being $T\epsilon\{R, L, U, B, N\}$ (depending on the Model) and the vector of regression coefficients of Model k associated with X_i^k and the posterior probability, respectively. Since, in multinomial logistic regression, the epileptogenic side Y_i for each observation in the training dataset was assumed to be known, the posterior probability $\Pr(Y_i = T|M_k)$ was set to 0 or 1 depending on the decision made for laterality. By estimation of coefficients β_T^k for Model k, the posterior probability of the epileptogenic side Y_j for the j^{th} validation data was calculated.

The comparative index of deviance (Dev) was calculated for the response models as a sum of squares of residuals between the maxima of the observed data and the fitted log likelihood functions. The smaller the deviance, the more accurate the model fits the training data. The probability of detection (PD), on the other hand, was calculated to posteriorly measure the performance of the model decision making on the test data. It was defined as:

$$PD = \frac{1}{n}\sum_{j=1}^{n}\sum_{T} 1(Y_j = T|Side_j = T) \quad (2)$$

where n is the number of all subjects and Y_j and $Side_j$ are the lateralization result and the epileptogenic side, respectively and 1(.) is a unit function with the value of 1 for true arguments and 0, otherwise.

We also compared the lateralization result by the proposed model M3 using neuroclinical and neuroimaging methods outlined here:

- Neuroclinical methods
  - EEG Phase I monitoring
  - WADA (i.e., intracarotid sodium amobarbital procedure) on both left and right hemispheres to establish cerebral language and memory representation of each hemisphere (Loring, 1997).
  - Neuropsychological tests of language, verbal, and nonverbal memory, and IQ (Akanuma et al., 2003; Jones-Gotman et al., 2010; Keary et al., 2007) including
    - Boston naming test
    - Wechsler verbal and nonverbal immediate and delayed memory tests
    - California verbal learning recognition, long delay free recall, and total tests
    - Rey–Osterreith nonverbal immediate and delayed memory
    - Verbal, nonverbal and full scale IQ tests.
- Neuroimaging asymmetry methods (Nazem-Zadeh et al., 2014b) including
  - FA in posteroinferior cingulum
  - FA in fornix
  - Hippocampal volume, hippocampal FLAIR intensity

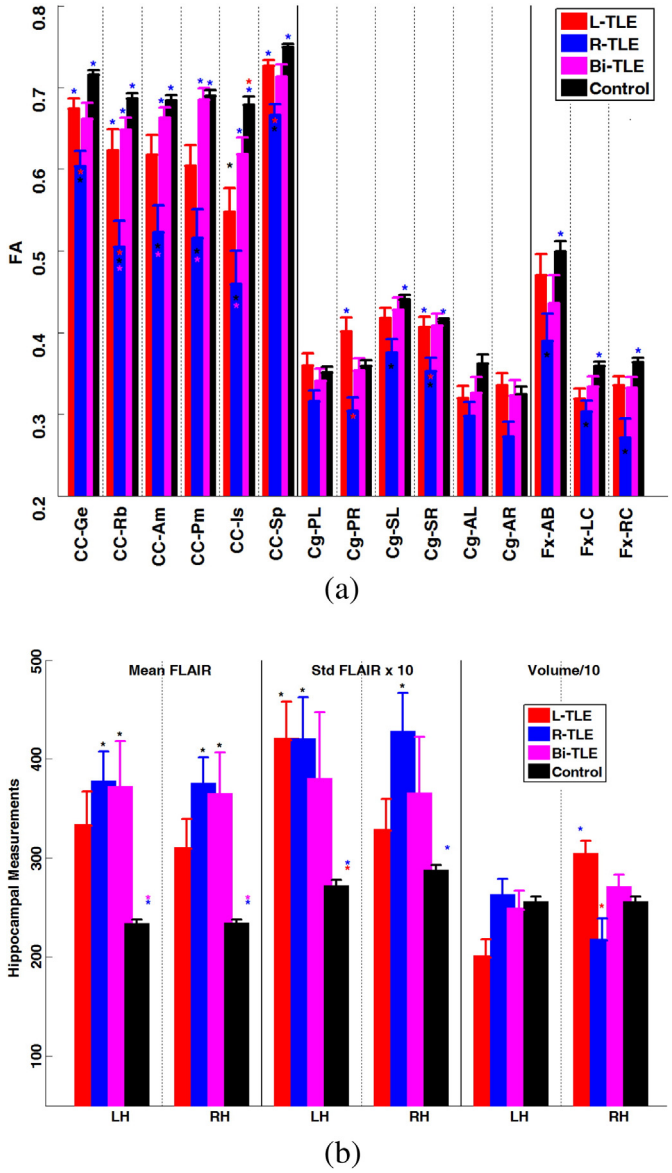

Fig. 2. Comparison of FA across the cingulum, corpus callosum and fornix (a) and the mean and standard deviation of hippocampal FLAIR intensities and volumes in the left and right hippocampi (b), between mTLE cohorts and the control cohort. Asterisks show significant differences in each cohort with respect to the other cohorts with the corresponding color, after Bonferroni adjustments. Note that, for greater clarification, the standard deviations of hippocampal FLAIR intensities and the hippocampal volumes have been scaled to ×10 and 1/10, respectively. Figure notations: FA: fractional anisotropy, Ge: genu, Rb: rostral body, Am: anterior midbody, Pm: posterior midbody, Is: isthmus, Sp: splenium of CC: corpus callosum. A: anteroinferior, S: superior, P: posteroinferior, L: left side, R: right side of Cg: cingulum. Ab: anterior body, LC: left crus, RC: right crus of Fx: fornix. Std: standard deviation, TLE: temporal lobe epilepsy, R, L, and Bi TLE: TLE patients with right, left, and bilateral epileptogenic side, respectively. LH and RH: left and right hippocampus, Std: standard deviation, FLAIR: Fluid Attenuated Inversion Recovery.

3. Results

3.1. Structural change

The patients averaged 10 years older than controls ($p = 0.001$), but was no significant difference in age by mTLE cohorts ($p = 0.436$). Gender proportions were statistically equivalent for the groups ($p > 0.31$). Two-way RMANOVA demonstrated significant interaction between region and mTLE laterality type in FA measurements ($p < 0.001$). Fig. 2a and Table 2 show the results of comparisons among the mTLE laterality types for each region using one-way ANOVA. For all callosal regions, right posteroinferior and bilateral superior cingulate regions, and bilateral forniceal crura, the overall ANOVA F-test on all mTLE laterality types was significant after Bonferroni adjustments ($p < 0.0024$). In the t-tests between pairs of laterality types, FA showed significant differences in all callosal subregions for right mTLE versus control, in the genu, rostral body, and splenium for right versus left mTLE, and in the rostral, anterior and posterior midbody, and isthmus for right versus bilateral mTLE. The callosal isthmus showed significant differences for left mTLE versus control cohort ($p < 0.0083$). In the t-tests between pairs of types, FA showed significant differences in bilateral superior cingulate subregions for right mTLE versus control, and in

Table 2
The comparison of FA and hippocampal measurements among the mTLE laterality types using one-way ANOVA and pairwise comparisons between laterality types.

			L mTLE vs. Control	R mTLE vs. Control	B mTLE vs. Control	L mTLE vs. B mTLE	R mTLE vs. B mTLE	L mTLE vs. R mTLE	Overall mTLE Effect (3 df)
FA measurements	Corpus Callosum	Ge	0.063	<0.001	0.040	0.939	0.050	0.002	<0.001
		Rb	0.080	<0.001	0.614	0.887	0.001	0.001	<0.001
		Am	0.055	<0.001	0.900	0.547	0.001	0.009	<0.001
		Pm	0.012	<0.001	0.999	0.120	<0.001	0.030	<0.001
		Is	<0.001	<0.001	0.407	0.360	0.003	0.085	<0.001
		Sp	0.156	<0.001	0.040	0.805	0.010	<0.001	<0.001
	Cingulum	PL	0.932	0.085	0.934	0.758	0.582	0.053	0.053
		PR	0.066	0.009	0.993	0.151	0.124	<0.001	<0.001
		SL	0.392	<0.001	0.893	0.946	0.043	0.068	<0.001
		SR	0.966	<0.001	0.988	1.000	0.017	0.005	<0.001
		AL	0.148	0.010	0.434	0.995	0.698	0.757	0.011
		AR	0.932	0.028	1.000	0.956	0.165	0.019	0.015
	Fornix	AB	0.790	0.005	0.344	0.839	0.680	0.118	0.008
		LC	0.016	<0.001	0.394	0.810	0.296	0.730	<0.001
		RC	0.347	<0.001	0.435	1	0.042	0.009	<0.001
Hippocampal measurements	FLAIR Mean	LH	0.015	<0.001	0.004	0.805	0.999	0.636	<0.001
		RH	0.048	<0.001	0.002	0.487	0.993	0.211	<0.001
	FLAIR Std	LH	0.004	0.004	0.144	0.884	0.886	1.000	<0.001
		RH	0.666	0.002	0.301	0.877	0.576	0.096	<0.001
	Volume	LH	0.019	0.976	0.991	0.197	0.938	0.020	0.014
		RH	0.045	0.159	0.904	0.502	0.134	0.001	0.001

The background shading and the numbers in cells represent, respectively, the significance and unadjusted p-values between pairs of left (L), right (R), and bilateral (B) mTLE, and control cohorts, for the overall mTLE effect (last column). Overall p-values were significant if below $0.05/21 = 0.0024$. Pairwise p-values were significant if below $0.05/6 = 0.0083$.
Table notations: FA: fractional anisotropy, Ge: genu, Rb: rostral body, Am: anterior midbody, Pm: posterior midbody, Is: isthmus, Sp: splenium of corpus callosum. A: anteroinferior, S: superior, P: posteroinferior, L: left side, R: right side of cingulum. AB: anterior body, LC: left crus, RC: right crus of fornix. Std: standard deviation, LH: left hippocampus, RH: right hippocampus. mTLE: mesial temporal lobe epilepsy, R, L, and B mTLE: mTLE patients with right, left, and bilateral epileptogenic side, respectively. FLAIR: Fluid Attenuated Inversion Recovery.

the right posteroinferior and right superior cingulate subregions for left and right mTLE ($p < 0.0083$). FA showed significant differences in all forniceal crura for right mTLE versus control ($p < 0.0083$).

Table 3 shows the results of one-way RMANOVA for the corpus callosum, cingulum, and fornix followed by paired t-tests between pairs of their subregions for each mTLE laterality type. The overall RMANOVA F-tests were significant across the entire corpus callosum, cingulum, and fornix ($p < 0.0028$), and for genu versus rostral body, posterior midbody versus isthmus, and isthmus versus splenium in corpus-callosum, for left superior versus right superior and for all neighboring structures in cingulum, and for all neighboring structures in fornix ($p < 0.0083$). Within the corpus callosum, a significant difference was observed between the isthmus and splenium for all cohorts, between the genu and rostral body for right mTLE and control cohorts, and between the posterior midbody and isthmus for right mTLE. For the neighboring structures of the cingulum, a significant difference was observed between the posteroinferior and superior and between the superior and anteroinferior subregions of both sides for all cohorts, except for the posteroinferior and superior right subregions in left mTLE cohort. For the cingulate corresponding bilateral structures, a significant difference was observed between left and right superior subregions for bilateral mTLE and control cohorts. For the fornix, a significant difference was observed between the anterior body and left crus for left mTLE and control, and between the anterior body and right crus for left mTLE, right mTLE, and control cohorts. The results for MD measurements were not significant.

Two-way RMANOVA showed significant interaction between region and mTLE laterality type for the hippocampal measurements ($p < 0.001$). Fig. 2b and Table 2 show the results of comparison among the mTLE laterality types for the left and right hippocampi using one-way ANOVA. For all hippocampal measurements except for the left hippocampal volume, the overall ANOVA F-test on all mTLE laterality types was significant after Bonferroni adjustments ($p < 0.0024$). In the t-tests between pairs of laterality types, the mean of FLAIR intensity in both hippocampi showed significant differences for right and bilateral mTLE versus control. Moreover, the standard deviation of FLAIR intensity in both hippocampi showed significant differences for right mTLE versus control, and in left hippocampus for left mTLE versus control. Furthermore, the right hippocampal volume showed a significant difference for left versus right mTLE ($p < 0.0083$).

3.2. Lateralization response-driven models

Based on the differences in FA in the corpus callosum, cingulum and fornix, multivariate response-driven models were developed as biomarkers of laterality, to determine what the simplest and most accurate methods were for distinguishing between unilateral and bilateral cases as well as to specify the laterality of individual mTLE cases. Table 4 shows the probability of detection and the deviance of the fit for Models 1 to 3, averaged over 54 repetitions of leave-one-out cross validations using the FA feature vectors in the cingulate, callosal, and forniceal subregions. In Model 1, the side of epileptogenicity was detected in 100% of cases of left and right mTLE only using the FA feature vector in the cingulum (Dev = 7.3). This demonstrates that the cingulum expresses greater asymmetry than either the fornix or corpus callosum in unilateral mTLE cases. Integrating the FA attribute into both corpus callosum and cingulum, the same probability of detection was achieved (100%) while drastically decreasing the deviance of the fit (Dev = 0.7), which implied a more accurate fit of the model to the dataset. By such integration, a 100% probability of detection was also achieved for Model 2. It can be inferred that the corpus callosum contributes considerably more than the cingulum or fornix for distinguishing bilateral from unilateral mTLE cases. The integration of forniceal FA features with both the corpus callosum and cingulum achieved a 100% probability of detection for Model 3, while assigning all cases correctly to each of the unilateral right and left mTLE, bilateral mTLE and control cohorts with a lower deviance for all Models (Dev = 30.4). The same 100% probability of detection for Model 3 is achieved by reducing the cingulate features to only left and right posteroinferior for a total 11 of features. The slight increase in the deviance of the fit (Dev = 36.6) may imply a lower chance of

Table 3
The results of FA comparison within three structures by RMANOVA, and among pairs of regions using paired t-tests.

			L mTLE	R mTLE	U mTLE	B mTLE	mTLE	Control	All Subjects
FA measurements	Corpus callosum	Entire structure	<0.001	<0.001	<0.001	<0.002	<0.001	<0.001	<0.001
		Ge vs. Rb	0.019	0.002	<0.001	0.46	<0.001	<0.001	<0.001
		Rb vs. Am	0.700	0.113	0.455	0.282	0.247	0.674	0.412
		Am vs. Pm	0.133	0.575	0.159	0.109	0.656	0.371	0.855
		Pm vs. Is	0.012	<0.001	<0.001	0.010	<0.001	0.174	<0.001
		Is vs. Sp	<0.001	<0.001	<0.001	0.008	<0.001	<0.001	<0.001
	Cingulum	Entire structure	<0.001	<0.001	<0.001	<0.001	<0.001	<0.001	<0.001
		PL vs. PR	0.002	0.269	0.119	0.323	0.065	0.106	0.017
		SL vs. SR	0.131	0.069	0.018	<0.001	<0.001	<0.001	<0.001
		AL vs. AR	0.240	0.203	0.677	0.700	0.626	0.015	0.029
		PL vs. SL	<0.001	0.002	<0.001	0.001	<0.001	<0.001	<0.001
		SL vs. AL	<0.001	<0.001	<0.001	<0.001	<0.001	<0.001	<0.001
		PR vs. SR	0.709	0.005	0.023	<0.001	<0.001	<0.001	<0.001
		SR vs. AR	<0.001	<0.001	<0.001	<0.001	<0.001	<0.001	<0.001
	Fornix	Entire structure	<0.001	<0.001	<0.001	0.005	<0.001	<0.001	<0.001
		AB vs. LC	<0.001	0.011	<0.001	0.021	<0.001	<0.001	<0.001
		AB vs. RC	<0.001	<0.001	<0.001	0.028	<0.001	<0.001	<0.001
		LC vs. RC	0.088	0.104	0.485	0.873	0.469	0.138	0.74

The background shading and the numbers in cells represent, respectively, the significance and unadjusted p-values between pairs of regions, including all adjacent subregions and corresponding left and right subregions in cingulum and fornix, for different cohorts of left, right, unilateral, bilateral, and all mTLE, control, and for all subjects together. The p-values (last column) were significant if below 0.05/18 = 0.0028. The p-values for specific mTLE groups were significant if below 0.05/6 = 0.0083.
Table notations: FA: fractional anisotropy, Ge: genu, Rb: rostral body, Am: anterior midbody, Pm: posterior midbody, Is: isthmus, Sp: splenium of corpus callosum. A: anteroinferior, S: superior, P: posteroinferior, L: left side, R: right side of cingulum. AB: anterior body, LC: left crus, RC: right crus of fornix. mTLE: patients with mesial temporal lobe epilepsy; R, L, U and B mTLE: mTLE patients with right, left, unilateral, and bilateral epileptogenic side, respectively.

overfitting and a higher generalization of the model to a new dataset. Fig. 3a and b shows the logistic fit for binomial Models 1 to 2 using the reduced FA feature vectors in the cingulate, callosal and forniceal subregions. The MD metric did not contribute to the solution as substantively as the FA metric.

The same multivariate response-driven models were developed from more standard volumetrics and FLAIR analyses as a comparison to DTI-based models. The combination of mean and standard deviation of hippocampal FLAIR intensities and hippocampal volumes was superior to any other combination (Table 4). Fig. 3c and d shows the logistic fit and the probability of detection for binomial Models 1 and 2 using all hippocampal features. The left and right mTLE cohorts were distinguishable from each other by Model 1. However, the bilateral cohort was not distinguishable from unilateral cohorts using Model 2. Even in models with PD = 1, a lower deviance was achieved with FA, suggesting a more appropriate fit with FA metrics than with those of the hippocampus.

Table 1 also shows the lateralization results by neuroclinical (columns 4–6) as well as neuroimaging methods (columns 11–15). Correct detection of mTLE laterality by each of these lateralization methods ranged widely as 24/31, 18/30, 15/27, 18/31, 22/31, 23/31, 22/31, and 31/31, respectively, considering that the results of some neuroclinical methods were not available. Some mTLE cases could not be lateralized by these other methods, with either false positive or nonlateralizing results obtained (Table 1).

Table 4
The probability of detection and the deviance of fit averaged over 54 repetitions of leave-one-out cross validation for lateralization models (columns), using feature vectors of FA measurements in the corpus callosum, cingulum, and fornix subregions and their combinations, as well as mean and standard deviation of hippocampal FLAIR intensities and volumes in the left and right hippocampi and their combinations (rows).

			M1	M2	M3
FA measurements	Corpus callosum	PD	0.96	0.87	0.76
		Dev	7.97	16.87	62.13
	Cingulum	PD	1.00	0.81	0.69
		Dev	7.41	25.28	86.87
	Fornix	PD	0.88	0.74	0.76
		Dev	20.68	26.74	89.98
	Corpus callosum + cingulum	PD	1.00	1.00	0.96
		Dev	0.67	12.35	40.75
	Corpus callosum + fornix	PD	1.00	0.97	0.91
		Dev	3.43	13.41	44.68
	Cingulum + fornix	PD	1.00	0.87	0.93
		Dev	4.41	19.46	59.13
	Corpus callosum + cingulum + fornix	PD	1.00	1.00	1.00
		Dev	0.11	10.84	30.36
	Reduced features corpus callosum + cingulum + fornix	PD	1.00	1.00	1.00
		Dev	2.8	14.23	36.54
Hippocampal measurements	FLAIR mean	PD	0.83	0.77	0.69
		Dev	23.01	32.28	95.12
	FLAIR Std	PD	0.79	0.77	0.61
		Dev	28.14	32.63	108.22
	FLAIR mean + FLAIR Std	PD	0.79	0.71	0.72
		Dev	20.65	30.12	80.07
	Volume	PD	0.92	0.77	0.72
		Dev	9.47	32.68	88.41
	FLAIR mean + FLAIR Std + volume	PD	1.00	0.71	0.81
		Dev	1.60	30.00	44.78

Table notations: FA: fractional anisotropy, PD: probability of detection, Dev: deviance of the fit, Std: standard deviation. FLAIR: Fluid Attenuated Inversion Recovery. M1–M3: lateralization Models 1 to 3. The background shading in cells represents 100% probability of detection achieved by models and features.

4. Discussion

The cingulum, fornix and corpus callosum were seen to have distinctive diffusion indices in cases of both unilateral and bilateral mTLE compared to that of control subjects sufficient to distinguish them from one another. We compared these DTI-based changes with hippocampal structural changes (i.e., volumetrics and FLAIR intensities) and found the former to be more reliable not simply in distinguishing between unilateral and bilateral mTLE cases but in specifying the laterality of individual mTLE cases. These were then used to develop a response-driven lateralization model that could be used as an effective quantitative neuroimaging biomarker to establish unilateral and bilateral epileptogenic zones in mTLE in order to lessen diagnostic ambiguity and, hopefully, eventually to reduce the need for invasive electrographic monitoring. The proposed lateralization model based on FA measurements was superior to neuroclinical methods including EEG Phase I monitoring, WADA, and neuropsychological tests as well as to previously introduced neuroimaging asymmetry analysis methods including FA in the posteroinferior cingulum and fornix, and hippocampal volume and FLAIR intensity. A combined model integrating the FA and hippocampal measurements would probably further improve the probability of detection in other datasets. Regression overfitting can be partly addressed by testing the model's ability to generalize its performance on a set of data not used for training by cross validation techniques, although overfitting can be a concern when the number of integrated features becomes comparable to the sample size.

Previous research has studied changes of DTI indices either in cases of mTLE or MTS compared to a nonepileptic cohort (Concha et al., 2009; Gross et al., 2006; Kim et al., 2008), or between brain structures ipsilateral and contralateral to the site of seizure onset (Concha et al., 2004, 2009; Liacu et al., 2012a; Nazem-Zadeh et al., 2014b). Only a few studies have compared DTI changes in cases of right and left mTLE (Ahmadi et al., 2009; Focke et al., 2008; McDonald et al., 2008; Shon et al., 2010). Focke et al. (2008) reported FA reduction in both left and right forniceal crura for right mTLE and in the left forniceal crus for left mTLE (Focke et al., 2008). These findings were supported by the current study, but only the former was significant. Otherwise, an FA reduction in the parahippocampal gyrus was not identified in our left mTLE cohort. Our finding in posteroinferior cingulum was in agreement with McDonald et al. (2008) who found that in parahippocampal cingulum, right mTLE patients showed a lower FA in the right side compared to the left, and left mTLE patients showed a lower FA in the left side compared to the right (McDonald et al., 2008). They found FA in the right parahippocampal cingulum significantly lower in the right mTLE patients compared to the controls. They did not find the fornix sensitive to mTLE laterality compared to controls. Shon et al. (2010) reported increased MD for mTLE cases with MTS in the ipsilateral hippocampus as well as the parahippocampal and frontoparietal regions. Those patients with a left MTS also, specifically, showed MD increases in the ipsilateral posterior cingulum and the callosal isthmus in addition to the contralateral occipitotemporal regions. In the absence of MTS, the left mTLE cases demonstrated increased MD in the ipsilateral posterior fornix and the posterior cingulum. They reported that changes in MD were more predominant and extensive in patients with left compared to patients with right mTLE (Shon et al., 2010). Ahmadi et al. (2009) reported reduced FA in the ipsilateral cingulate and parahippocampal gyri in cases of right and left TLE (Ahmadi et al., 2009). Significant fiber tract asymmetry was evident in cases of right TLE with reduced FA in the right inferior fronto-occipital fasciculus and fasciculi of the parahippocampal and cingulate gyri. Those with left TLE demonstrated reduced FA in the left fornix

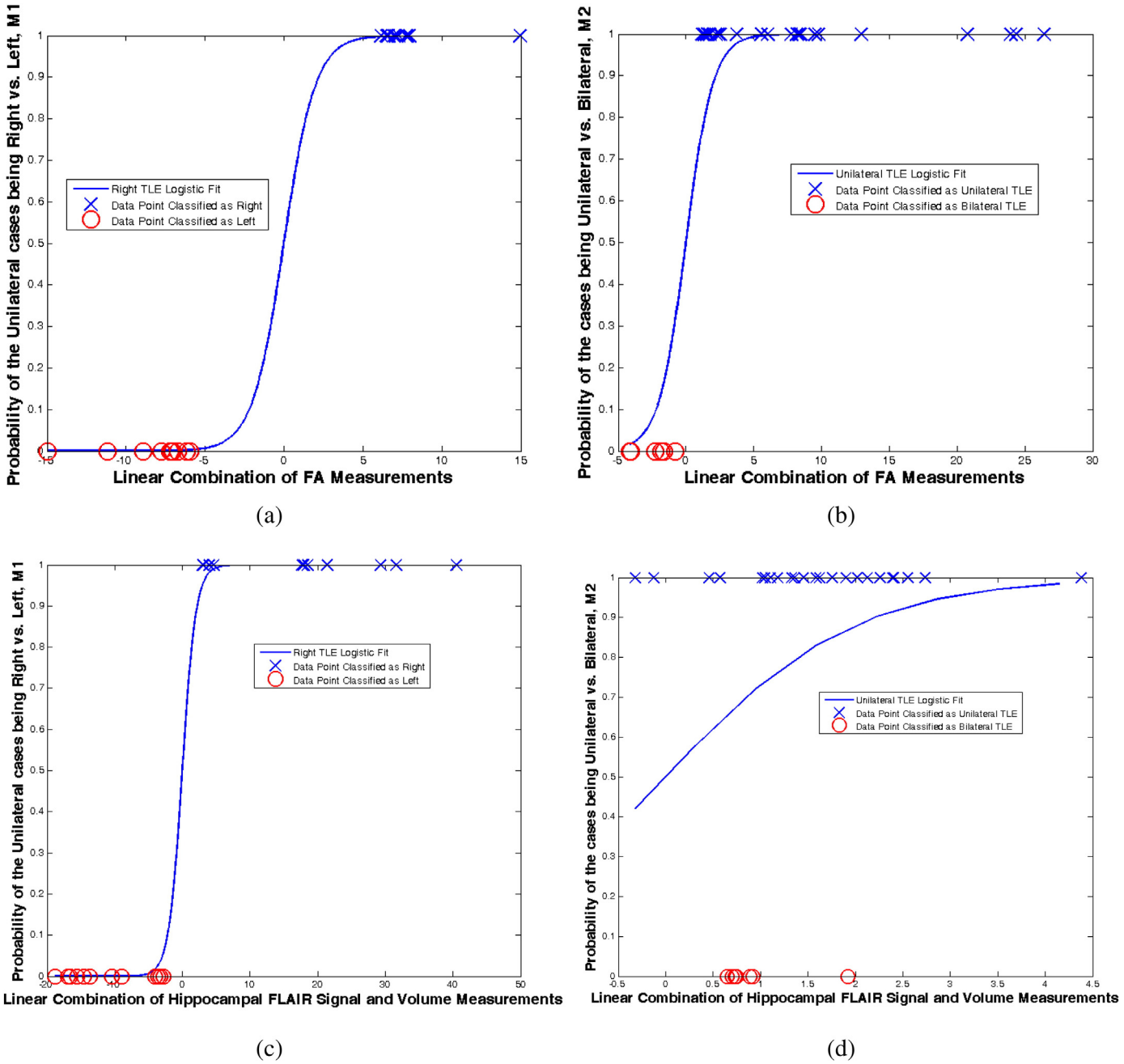

Fig. 3. The logistic fit and the probability of detection for Models 1 and 2 using the features vector of FA measurements in the cingulum, corpus callosum, and fornix subregions (a and b, respectively), as well as the features vector of FLAIR signal intensity and volume measurements in the hippocampus (c and d, respectively). FA: fractional anisotropy, TLE: temporal lobe epilepsy. FLAIR: Fluid Attenuated Inversion Recovery. Note that each curve is the average of 54 curves generated by repetitions of leave-one-out cross validation.

relative to the right. Similar trends were seen in the present study as for the cingulum and fornix but were not judged significant. Ahmadi et al. (2009) also found general bilateral widespread white matter changes in patients with left mTLE and mostly unilateral changes in patient with right mTLE compared to controls. In contrast, we found the right mTLE patients underwent more FA reduction in corpus callosum, cingulum, and fornix subregions than left and bilateral mTLE cohorts, compared to the control cohort. Because of the variability in diffusion properties seen across the cingulum, it may be best to consider division of this structure into superior, posteroinferior, and anteroinferior subregions to better appreciate distinct DTI changes in cases of mTLE (Nazem-Zadeh et al., 2014b).

In this work, we studied the diffusion anisotropy in the fornix, cingulum and corpus callosum as the white matter structures affected by mTLE evidenced in the literature. We were also interested in studying other fiber tracts such as uncinate fasciculus and hippocampal mossy fibers, which, however, cannot be reconstructed accurately and reproducibly using streamline fiber tracking methods. Tract-based spatial statistics (TBSS) methods were not intended to be utilized either, because instead of measuring the anisotropy within the whole volume of white matter structures, they measure it across their skeleton or main axis. Furthermore, the atlas-based registration/segmentation methods do not work very well for quite small or narrow white matter structures as they are vulnerable to the misregistration between subjects.

Especially for some mTLE cases in which some of white matter structures do not align well with the atlas structures, uncertainty would be induced in feature measurements.

There are limited studies on the application of DTI indices for lateralizing seizure onset in individual mTLE patients. In our previous work, the problem of lateralization of mTLE was addressed by interhemispheric asymmetry analysis of FA in bilateral structures such as the posteroinferior cingula, forniceal crura, and hippocampi, where mTLE cohort showed a significant asymmetry in FA in ipsilateral compared to contralateral sides. However, the introduced asymmetry analysis could not detect the side of epileptogenicity in all non-MTS cases (Nazem-Zadeh et al., 2014b). In contrast, we included the corpus callosum and its subregions in the current study. The corpus callosum is a commissural fiber tract with diffusivity perpendicular to its main axis, which it does not contain bilateral structures to apply the asymmetry analysis. Furthermore, significant interhemispheric variation of FA for either the cingulum or the forniceal crura in any mTLE cohorts was not evident. Paired measures establishing single asymmetry indices were therefore not worthwhile. In addition to the problem of identifying the mTLE laterality, the current study addresses the problem of distinguishing unilateral from bilateral mTLE, using FA metrics in the subregions of the cingulum, fornix and corpus callosum. The proposed model was not only successful in detecting all bilateral mTLE cases but effectively identified the side of epileptogenicity for all unilateral non-MTS mTLE cases. It also was capable of rendering the probability of unilateral or bilateral epileptogenicity and the side of epileptogenicity in the case of unilateral mTLE.

In the current study, the variability in quantitative imaging indices was alleviated through the use of a single imaging scanner with identical parameters. Subject-specific factors related to the natural variability of neurobiological attributes in designated anatomical sites were taken into account by integrating the indices of a nonepileptic control cohort and multinomial modeling, establishing boundary domains from the nonepileptic cohort as a means of defining acceptable ranges (Nazem-Zadeh et al., 2014a). This provided greater confidence in determining laterality for those cases whose imaging attributes were identified as existing outside the boundary domain.

Some limitations exist in the current study. The number of bilateral mTLE patients reviewed was not large. The further recruitment of bilateral cases over time will provide greater assurance of these findings in order to implement a robust lateralization scheme. The proposed lateralization model is only applicable to stringently defined mTLE patients and is not generalizable to all epilepsy patients. It is not likely to be valid for patients with suspected extratemporal epilepsy. The validity in patients with lateral, neocortical TLE is unknown. Due to the variability of DTI indices inherent in the choice of scanner and imaging parameters, the model is also only applicable to those patients imaged by the scanner and imaging parameters for which the model has been developed. Finally, even for the same imaging system, further steps, such as validation in an independent cohort of patients is called for before clinical application.

The use of icEEG allowed establishment of bilateral TLE as those with truly independent bitemporal ictal origins. Despite electrographic features supporting bilateral independent temporal epileptogenicity, there have been efforts by several groups to assess predominance of one side over the other, leading to considerations of surgical candidacy (Boling et al., 2009; Chung et al., 1991; Hirsch et al., 1991; Holmes et al., 2003; Luo et al., 2013; Malmgren et al., 2014; Sirven et al., 1997). In a review of bitemporal epileptogenicity, Aghakhani et al. (2014) evaluated group data of those cases declared to express genuine bitemporal epileptogenicity by extraoperative icEEG. Out of 173 bitemporal patients who were found to have sufficient laterality and underwent unilateral resection, 58 patients (33.5%) achieved Engel class I and 19 patients (11%) achieved Engel class II outcomes. Zhang et al. (2014) reported 41.7% of patients with bilateral mTLE, 50% of whom were MRI-negative, became seizure-free (Zhang et al., 2014). Spencer et al. (2011) questioned the notion that icEEG for 1 to 3 weeks should be considered the gold standard. They suggested that some of the failures in resection of putative epileptic foci in presumed unilateral patients may be due to the fact that certain numbers of patients are truly bilateral. There may be a sampling error attributable to an insufficiently short-term icEEG. They averred that icEEG with NeuroPace RNS™ is probably the gold standard (Spencer et al., 2011). Nevertheless based on these comprehensive studies, the reliance on icEEG alone as a necessarily strong or exclusive predictor of surgical outcome for apparent bilateral mTLE cases may not be fully warranted (Aghakhani et al., 2014). A multimodal approach including neuroimaging and icEEG can identify an epileptic focus in most cases, and provide suitable surgical options for nonlesional or bilateral mTLE patients with a possible good outcome (Zhang et al., 2014). The notion that DTI attributes may have a declarative role is compelling because of the overt structural changes putatively brought about by epileptogenicity. Such DTI changes in bilateral mTLE patients, if concordant with icEEG, may be sufficiently robust to serve as a suitable differentiating metric or biomarker, to more confidently proceed with a unilateral resection.

5. Conclusions

By looking at the DTI characteristics of various brain regions, we were able to differentiate 12 left, 12 right and 7 bilateral mTLE from one another and from 23 controls more robustly than with a model using more traditional volumetrics and FLAIR analyses of the hippocampus. This pilot study suggests that the application of the proposed lateralization model on a large population of mTLE cases may further prove its ability in lessening the diagnostic ambiguity of laterality and help optimize selection of surgical candidates.

Funding statement

This work was supported in part by NIH grant R01-EB013227.

Ethics approval

Ethics approval was provided by Henry Ford Health System Institutional Review Board, Detroit, Michigan, USA.

Conflict of interest

There is no conflict of interest to report.

Acknowledgments

Special thanks to Mario Darvishi and Harrini Vijay for their invaluable help in data processing.

References

Achten, E., Boon, P., Van De Kerckhove, T., Caemaert, J., De Reuck, J., Kunnen, M., 1997. Value of single-voxel proton MR spectroscopy in temporal lobe epilepsy. Am. J. Neuroradiol. 18, 1131–1139.

Aghakhani, Y., Liu, X., Jette, N., Wiebe, S., 2014. Epilepsy surgery in patients with bilateral temporal lobe seizures: a systematic review. Epilepsia 55 (12), 1892–1901.

Ahmadi, M.E., Hagler, D., McDonald, C.R., Tecoma, E., Iragui, V., Dale, A.M., Halgren, E., 2009. Side matters: diffusion tensor imaging tractography in left and right temporal lobe epilepsy. Am. J. Neuroradiol. 30, 1740–1747.

Akanuma, N., Alarcon, G., Lum, F., Kissani, N., Koutroumanidis, M., Adachi, N., Binnie, C.D., Polkey, C.E., Morris, R.G., 2003. Lateralising value of neuropsychological protocols for presurgical assessment of temporal lobe epilepsy. Epilepsia 44, 408–418.

Akhondi-Asl, A., Jafari-Khouzani, K., Elisevich, K., Soltanian-Zadeh, H., 2011. Hippocampal volumetry for lateralization of temporal lobe epilepsy: automated versus manual methods. Neuroimage 54, S218–S226.

Aroniadou-Anderjaska, V., Fritsch, B., Qashu, F., Braga, M.F., 2008. Pathology and pathophysiology of the amygdala in epileptogenesis and epilepsy. Epilepsy Res. 78, 102–116.

Arya, R., Mangano, F.T., Horn, P.S., Holland, K.D., Rose, D.F., Glauser, T.A., 2013. Adverse events related to extraoperative invasive EEG monitoring with subdural grid electrodes: a systematic review and meta-analysis. Epilepsia 54, 828–839.

Bernasconi, N., Bernasconi, A., Andermann, F., Dubeau, F., Feindel, W., Reutens, D., 1999. Entorhinal cortex in temporal lobe epilepsy: a quantitative MRI study. Neurology 52 (9), 1870-1870.
Bernasconi, N., Bernasconi, A., Caramanos, Z., Antel, S., Andermann, F., Arnold, D., 2003. Mesial temporal damage in temporal lobe epilepsy: a volumetric MRI study of the hippocampus, amygdala and parahippocampal region. Brain 126, 462–469.
Boling, W., Aghakhani, Y., Andermann, F., Sziklas, V., Olivier, A., 2009. Surgical treatment of independent bitemporal lobe epilepsy defined by invasive recordings. J. Neurol. Neurosurg. Psychiatry 80, 533–538.
Bonilha, L., Nesland, T., Martz, G.U., Joseph, J.E., Spampinato, M.V., Edwards, J.C., Tabesh, A., 2012. Medial temporal lobe epilepsy is associated with neuronal fibre loss and paradoxical increase in structural connectivity of limbic structures. J. Neurol. Neurosurg. Psychiatry 83 (9), 903–909.
Bulacio, J.C., Jehi, L., Wong, C., Gonzalez-Martinez, J., Kotagal, P., Nair, D., Najm, I., Bingaman, W., 2012. Long-term seizure outcome after resective surgery in patients evaluated with intracranial electrodes. Epilepsia 53, 1722–1730.
Chahboune, H., Mishra, A.M., DeSalvo, M.N., Staib, L.H., Purcaro, M., Scheinost, D., Papademetris, X., Fyson, S., Lorincz, M., Crunelli, V., 2009. DTI abnormalities in anterior corpus callosum of rats with spike–wave epilepsy. Neuroimage 47, 459–466.
Chiang, S., Haneef, Z., 2014. Graph theory findings in the pathophysiology of temporal lobe epilepsy. Clin. Neurophysiol. 125, 1295–1305.
Chung, M.Y., Walczak, T.S., Lewis, D.V., Dawson, D.V., Radtke, R., 1991. Temporal lobectomy and independent bitemporal interictal activity: what degree of lateralization is sufficient? Epilepsia 32, 195–201.
Concha, L., Beaulieu, C., Collins, D.L., Gross, D.W., 2009. White-matter diffusion abnormalities in temporal-lobe epilepsy with and without mesial temporal sclerosis. J. Neurol. Neurosurg. Psychiatry 80, 312–319.
Concha, L., Beaulieu, C., Gross, D.W., 2004. Bilateral limbic diffusion abnormalities in unilateral temporal lobe epilepsy. Ann. Neurol. 57, 188–196.
Concha, L., Gross, D.W., Beaulieu, C., 2005. Diffusion tensor tractography of the limbic system. Am. J. Neuroradiol. 26, 2267–2274.
Concha, L., Livy, D.J., Beaulieu, C., Wheatley, B.M., Gross, D.W., 2010. In vivo diffusion tensor imaging and histopathology of the fimbria-fornix in temporal lobe epilepsy. J. Neurosci. 30, 996–1002.
de Curtis, M., Paré, D., 2004. The rhinal cortices: a wall of inhibition between the neocortex and the hippocampus. Prog. Neurobiol. 74, 101–110.
de Tisi, J., Bell, G.S., Peacock, J.L., McEvoy, A.W., Harkness, W.F., Sander, J.W., Duncan, J.S., 2011. The long-term outcome of adult epilepsy surgery, patterns of seizure remission, and relapse: a cohort study. Lancet 378, 1388–1395.
DeSalvo, M.N., Douw, L., Tanaka, N., Reinsberger, C., Stufflebeam, S.M., 2014. Altered structural connectome in temporal lobe epilepsy. Radiology 270, 842–848.
Dupont, S., Samson, Y., Nguyen-Michel, V.H., Zavanone, C., Navarro, V., Baulac, M., Adam, C., 2015. Lateralizing value of semiology in medial temporal lobe epilepsy. Acta Neurol. Scand. 132 (6), 401–409.
Engel Jr., J., 1996. Surgery for seizures. N. Engl. J. Med. 334, 647–653.
Eriksson, S., Rugg-Gunn, F., Symms, M., Barker, G., Duncan, J., 2001. Diffusion tensor imaging in patients with epilepsy and malformations of cortical development. Brain 124, 617–626.
Firat, A., Tascioglu, A., Demiryurek, M., Saygi, S., Oguz, K.K., Tezer, F., Hayran, M., 2014. Evaluation of corpus callosum morphometry in patients with mesial temporal lobe epilepsy with hippocampal sclerosis. Surg. Radiol. Anat. 36, 47–54.
Focke, N.K., Yogarajah, M., Bonelli, S.B., Bartlett, P.A., Symms, M.R., Duncan, J.S., 2008. Voxel-based diffusion tensor imaging in patients with mesial temporal lobe epilepsy and hippocampal sclerosis. Neuroimage 40, 728–737.
Gross, D.W., Concha, L., Beaulieu, C., 2006. Extratemporal white matter abnormalities in mesial temporal lobe epilepsy demonstrated with diffusion tensor imaging. Epilepsia 47, 1360–1363.
Hermann, B., Hansen, R., Seidenberg, M., Magnotta, V., O'Leary, D., 2003. Neurodevelopmental vulnerability of the corpus callosum to childhood onset localization-related epilepsy. Neuroimage 18, 284–292.
Hirsch, L.J., Spencer, S.S., Spencer, D.D., Williamson, P.D., Mattson, R.H., 1991. Temporal lobectomy in patients with bitemporal epilepsy defined by depth electroencephalography. Ann. Neurol. 30, 347–356.
Hirtz, D., Thurman, D., Gwinn-Hardy, K., Mohamed, M., Chaudhuri, A., Zalutsky, R., 2007. How common are the "common" neurologic disorders? Neurology 68, 326–337.
Holmes, M.D., Miles, A.N., Dodrill, C.B., Ojemann, G.A., Wilensky, A.J., 2003. Identifying potential surgical candidates in patients with evidence of bitemporal epilepsy. Epilepsia 44, 1075–1079.
Hosmer Jr., D.W., Lemeshow, S., Sturdivant, R.X., 2013. Applied logistic regression. Wiley.com.
Hufnagel, A., Elger, C.E., Pels, H., Zentner, J., Wolf, H.K., Schramm, J., Wiestler, O.D., 1994. Prognostic significance of ictal and interictal epileptiform activity in temporal lobe epilepsy. Epilepsia 35, 1146–1153.
Hufnagel, A., Weber, J., Marks, S., Ludwig, T., De Greiff, A., Leonhardt, G., Widmann, G., Stolke, D., Forsting, M., 2003. Brain diffusion after single seizures. Epilepsia 44, 54–63.
Hugg, J.W., Butterworth, E.J., Kuzniecky, R.I., 1999. Diffusion mapping applied to mesial temporal lobe epilepsy: preliminary observations. Neurology 53 (1) 173–173.
Jafari-Khouzani, K., Elisevich, K., Patel, S., Smith, B., Soltanian-Zadeh, H., 2010. FLAIR signal and texture analysis for lateralizing mesial temporal lobe epilepsy. Neuroimage 49, 1559–1571.
Jafari-Khouzani, K., Elisevich, K.V., Patel, S., Soltanian-Zadeh, H., 2011. Dataset of magnetic resonance images of nonepileptic subjects and temporal lobe epilepsy patients for validation of hippocampal segmentation techniques. Neuroinformatics 9, 335–346.
Jafari-Khouzani, K., Soltanian-Zadeh, H., Elisevich, K., 2006. Hippocampus volume and texture analysis for temporal lobe epilepsy. Electro/information Technology, 2006 IEEE International Conference on. IEEE, pp. 394–397.
Javidan, M., 2012. Electroencephalography in mesial temporal lobe epilepsy: a review. Epilepsy Res. Treat. 2012.
Jenkinson, M., Bannister, P., Brady, M., Smith, S., 2002. Improved optimization for the robust and accurate linear registration and motion correction of brain images. Neuroimage 17, 825–841.
Jones-Gotman, M., Smith, M.L., Risse, G.L., Westerveld, M., Swanson, S.J., Giovagnoli, A.R., Lee, T., Mader-Joaquim, M.J., Piazzini, A., 2010. The contribution of neuropsychology to diagnostic assessment in epilepsy. Epilepsy Behav. 18, 3–12.
Keary, T.A., Frazier, T.W., Busch, R.M., Kubu, C.S., Iampietro, M., 2007. Multivariate neuropsychological prediction of seizure lateralization in temporal epilepsy surgical cases. Epilepsia 48, 1438–1446.
Kim, C.H., Koo, B.B., Chung, C.K., Lee, J.M., Kim, J.S., Lee, S.K., 2010. Thalamic changes in temporal lobe epilepsy with and without hippocampal sclerosis: a diffusion tensor imaging study. Epilepsy Res. 90, 21.
Kim, H., Piao, Z., Ping, L., Bingaman, W., Dieht, B., 2008. Secondary white matter degeneration of the corpus callosum in patients with intractable temporal lobe epilepsy: a diffusion tensor imaging study. Epilepsy Res. 81, 136–142.
Kuba, R., Rektor, I., Brázdil, M., 2003. Ictal limb dystonia in temporal lobe epilepsy. An invasive video-EEG finding. Eur. J. Neurol. 10, 641–649.
Kuo, L.-W., Lee, C.-Y., Chen, J.-H., Wedeen, V.J., Chen, C.-C., Liou, H.-H., Tseng, W.-Y.I., 2008. Mossy fiber sprouting in pilocarpine-induced status epilepticus rat hippocampus: a correlative study of diffusion spectrum imaging and histology. Neuroimage 41, 789–800.
Kuzniecky, R., Bilir, E., Gilliam, F., Faught, E., Palmer, C., Morawetz, R., Jackson, G., 1997. Multimodality MRI in mesial temporal sclerosis: relative sensitivity and specificity. Neurology 49, 774–778.
Laitinen, T., Sierra, A., Pitkänen, A., Gröhn, O., 2010. Diffusion tensor MRI of axonal plasticity in the rat hippocampus. Neuroimage 51, 521–530.
Le Bihan, D., Breton, E., Lallemand, D., Grenier, P., Cabanis, E., Laval-Jeantet, M., 1986. MR imaging of intravoxel incoherent motions: application to diffusion and perfusion in neurologic disorders. Radiology 161, 401–407.
Liacu, D., Idy-Peretti, I., Ducreux, D., Bouilleret, V., de Marco, G., 2012a. Diffusion tensor imaging tractography parameters of limbic system bundles in temporal lobe epilepsy patients. J. Magn. Reson. Imaging 36, 561–568.
Liacu, D., Idy-Peretti, I., Ducreux, D., Bouilleret, V., de Marco, G., 2012b. Diffusion tensor imaging tractography parameters of limbic system bundles in temporal lobe epilepsy patients. J. Magn. Reson. Imaging 36 (3), 561–568.
Liu, M., Chen, Z., Beaulieu, C., Gross, D.W., 2014. Disrupted anatomic white matter network in left mesial temporal lobe epilepsy. Epilepsia 55 (5), 674–682.
Liu, M., Concha, L., Lebel, C., Beaulieu, C., Gross, D.W., 2012. Mesial temporal sclerosis is linked with more widespread white matter changes in temporal lobe epilepsy. Neuroimage Clin. 1, 99–105.
Loesch, A.M., Feddersen, B., Tezer, I.F., Hartl, E., Rémi, J., Vollmar, C., Noachtar, S., 2014. Seizure semiology identifies patients with bilateral temporal lobe epilepsy. Epilepsy Res. 109, 197–202.
Loring, D.W., 1997. Neuropsychological evaluation in epilepsy surgery. Epilepsia 38, S18–S23.
Luo, H., Zhao, Q., Tian, Z., Wu, Z., Wang, F., Lin, H., Yin, F., Zhao, H., Xiao, X., Yu, X., 2013. Bilateral stereotactic radiofrequency amygdalohippocampectomy for a patient with bilateral temporal lobe epilepsy. Epilepsia 54, e155–e158.
Malmgren, K., Rydenhag, B., Baxendale, S., Thompson, P.J., Duncan, J.S., Shorvon, S., Helmstaedter, C., Elger, C.E., 2014. Concerns about bilateral radiosurgical treatment of a patient with bilateral temporal lobe epilepsy. Epilepsia 55 (4) 623–623.
Mansouri, A., Fallah, A., Valiante, T.A., 2012. Determining surgical candidacy in temporal lobe epilepsy. Epilepsy Res. Treat. 2012.
Marks, W.J., Laxer, K.D., 1998. Semiology of temporal lobe seizures: value in lateralizing the seizure focus. Epilepsia 39, 721–726.
McDonald, C., Ahmadi, M., Hagler, D., Tecoma, E., Iragui, V., Gharapetian, L., Dale, A., Halgren, E., 2008. Diffusion tensor imaging correlates of memory and language impairments in temporal lobe epilepsy. Neurology 71, 1869–1876.
Mishra, A.M., Bai, H., Gribizis, A., Blumenfeld, H., 2011. Neuroimaging biomarkers of epileptogenesis. Neurosci. Lett. 497, 194–204.
Nakasu, Y., Nakasu, S., Morikawa, S., Uemura, S., Inubushi, T., Handa, J., 1995. Diffusion-weighted MR in experimental sustained seizures elicited with kainic acid. Am. J. Neuroradiol. 16, 1185–1192.
Nazem-Zadeh, M.-R., Chapman, C.H., Lawrence, T.S., Tsien, C.I., Cao, Y., 2013. Uncertainty in assessment of radiation-induced diffusion index changes in individual patients. Phys. Med. Biol. 58, 4277–4296.
Nazem-Zadeh, M.-R., Elisevich, K.V., Schwalb, J.M., Bagher-Ebadian, H., Mahmoudi, F., Soltanian-Zadeh, H., 2014a. Lateralization of temporal lobe epilepsy by multimodal multinomial hippocampal response-driven models. J. Neurol. Sci. 347, 107–118.
Nazem-Zadeh, M.-R., Schwalb, J.M., Elisevich, K.V., Bagher-Ebadian, H., Hamidian, H., Akhondi-Asl, A.-R., Jafari-Khouzani, K., Soltanian-Zadeh, H., 2014b. Lateralization of temporal lobe epilepsy using a novel uncertainty analysis of MR diffusion in hippocampus, cingulum, and fornix, and hippocampal volume and FLAIR intensity. J. Neurol. Sci. 342, 152–161.
Nazem-Zadeh, M.R., Chapman, C.H., Lawrence, T.L., Tsien, C.I., Cao, Y., 2012a. Radiation therapy effects on white matter fiber tracts of the limbic circuit. Med. Phys. 39, 5603–5613.
Nazem-Zadeh, M.R., Saksena, S., Babajani-Fermi, A., Jiang, Q., Soltanian-Zadeh, H., Rosenblum, M., Mikkelsen, T., Jain, R., 2012b. Segmentation of corpus callosum using diffusion tensor imaging: validation in patients with glioblastoma. BMC Med. Imaging 12, 10.
Pacia, S.V., Ebersole, J.S., 1999. Intracranial EEG in temporal lobe epilepsy. J. Clin. Neurophysiol. 16, 399.
Parekh, M.B., Carney, P.R., Sepulveda, H., Norman, W., King, M., Mareci, T.H., 2010. Early MR diffusion and relaxation changes in the parahippocampal gyrus precede the onset of spontaneous seizures in an animal model of chronic limbic epilepsy. Exp. Neurol. 224, 258–270.
Pereira, P.M.G., Insausti, R., Artacho-Pérula, E., Salmenperä, T., Kälviäinen, R., Pitkänen, A., 2005. MR volumetric analysis of the piriform cortex and cortical amygdala in drug-refractory temporal lobe epilepsy. Am. J. Neuroradiol. 26, 319–332.
Picard, R.R., Cook, R.D., 1984. Cross-validation of regression models. J. Am. Stat. Assoc. 79, 575–583.
Pierpaoli, C., Barnett, A., Pajevic, S., Chen, R., Penix, L.R., Virta, A., Basser, P., 2001. Water diffusion changes in Wallerian degeneration and their dependence on white matter architecture. Neuroimage 13, 1174–1185.
Pittau, F., Grova, C., Moeller, F., Dubeau, F., Gotman, J., 2012. Patterns of altered functional connectivity in mesial temporal lobe epilepsy. Epilepsia 53, 1013–1023.
Powell, H., Parker, G.J., Alexander, D.C., Symms, M.R., Boulby, P.A., Wheeler-Kingshott, C.A., Barker, G.J., Koepp, M.J., Duncan, J.S., 2007. Abnormalities of language networks in temporal lobe epilepsy. Neuroimage 36, 209–221.
Řehulka, P., Doležalová, I., Janoušová, E., Tomášek, M., Marusič, P., Brázdil, M., Kuba, R., 2014. Ictal and postictal semiology in patients with bilateral temporal lobe epilepsy. Epilepsy Behav. 41, 40–46.

Rodrigo, S., Oppenheim, C., Chassoux, F., Golestani, N., Cointepas, Y., Poupon, C., Semah, F., Mangin, J.-F., Le Bihan, D., Meder, J.-F., 2007. Uncinate fasciculus fiber tracking in mesial temporal lobe epilepsy. Initial findings. Eur. Radiol. 17, 1663–1668.

Rugg-Gunn, F., Eriksson, S., Symms, M., Barker, G., Duncan, J., 2001. Diffusion tensor imaging of cryptogenic and acquired partial epilepsies. Brain 124, 627–636.

Scanlon, C., Mueller, S.G., Cheong, I., Hartig, M., Weiner, M.W., Laxer, K.D., 2013. Grey and white matter abnormalities in temporal lobe epilepsy with and without mesial temporal sclerosis. J. Neurol. 260, 2320–2329.

Serles, W., Caramanos, Z., Lindinger, G., Pataraia, E., Baumgartner, C., 2000. Combining ictal surface-electroencephalography and seizure semiology improves patient lateralization in temporal lobe epilepsy. Epilepsia 41, 1567–1573.

Shon, Y.M., Kim, Y.I., Koo, B.B., Lee, J.M., Kim, H.J., Kim, W.J., Ahn, K.J., Yang, D.W., 2010. Group-specific regional white matter abnormality revealed in diffusion tensor imaging of medial temporal lobe epilepsy without hippocampal sclerosis. Epilepsia 51, 529–535.

Sirven, J.I., Malamut, B.L., Liporace, J.D., O'Connor, M.J., Sperling, M.R., 1997. Outcome after temporal lobectomy in bilateral temporal lobe epilepsy. Ann. Neurol. 42, 873–878.

Skudlarski, P., Jagannathan, K., Calhoun, V.D., Hampson, M., Skudlarska, B.A., Pearlson, G., 2008. Measuring brain connectivity: diffusion tensor imaging validates resting state temporal correlations. Neuroimage 43, 554–561.

So, N., Gloor, P., Quesney, L.F., Jones-Gotman, M., Olivier, A., Andermann, F., 1989. Depth electrode investigations in patients with bitemporal epileptiform abnormalities. Ann. Neurol. 25, 423–431.

Spencer, D., Gwinn, R., Salinsky, M., O'Malley, J.P., 2011. Laterality and temporal distribution of seizures in patients with bitemporal independent seizures during a trial of responsive neurostimulation. Epilepsy Res. 93, 221–225.

Sperling, M., O'Connor, M., Saykin, A., Phillips, C., Morrell, M., Bridgman, P., French, J., Gonatas, N., 1992. A noninvasive protocol for anterior temporal lobectomy. Neurology 42, 416-416.

Szabo, K., Poepel, A., Pohlmann-Eden, B., Hirsch, J., Back, T., Sedlaczek, O., Hennerici, M., Gass, A., 2005. Diffusion-weighted and perfusion MRI demonstrates parenchymal changes in complex partial status epilepticus. Brain 128, 1369–1376.

Thivard, L., Lehéricy, S., Krainik, A., Adam, C., Dormont, D., Chiras, J., Baulac, M., Dupont, S., 2005. Diffusion tensor imaging in medial temporal lobe epilepsy with hippocampal sclerosis. Neuroimage 28, 682–690.

Vaessen, M.J., Jansen, J.F., Vlooswijk, M.C., Hofman, P.A., Majoie, H.M., Aldenkamp, A.P., Backes, W.H., 2011. White matter network abnormalities are associated with cognitive decline in chronic epilepsy. Cereb. Cortex bhr298.

Vainio, P., Usenius, J., Vapalahti, M., Partanen, K., Kalviainen, R., Rinne, J., Kauppinen, R., 1994. Reduced N-acetylaspartate concentration in the temporal lobe epilepsy by quantitative 1H MRS in vivo. NeuroReport Int. J. Rapid Commun. Res. Neurosci. 5, 1733–1736.

Waites, A.B., Briellmann, R.S., Saling, M.M., Abbott, D.F., Jackson, G.D., 2006. Functional connectivity networks are disrupted in left temporal lobe epilepsy. Ann. Neurol. 59, 335–343.

Wall, C.J., Kendall, E.J., Obenaus, A., 2000. Rapid alterations in diffusion-weighted images with anatomic correlates in a rodent model of status epilepticus. Am. J. Neuroradiol. 21, 1841–1852.

Weber, B., Luders, E., Faber, J., Richter, S., Quesada, C.M., Urbach, H., Thompson, P.M., Toga, A.W., Elger, C.E., Helmstaedter, C., 2007. Distinct regional atrophy in the corpus callosum of patients with temporal lobe epilepsy. Brain 130, 3149–3154.

Wieshmann, U.C., Symms, M.R., Barker, G.J., Birnie, K.D., Shorvon, S.D., 1999. Water diffusion in the human hippocampus in epilepsy. Magn. Reson. Imaging 17, 29–36.

Witelson, S.F., 1989. Hand and sex differences in the isthmus and genu of the human corpus callosum. A postmortem morphological study. Brain 112, 799–835.

Yang, P.-F., Pei, J.-S., Zhang, H.-J., Lin, Q., Mei, Z., Zhong, Z.-H., Tian, J., Jia, Y.-Z., Chen, Z.-Q., Zheng, Z.-Y., 2014. Long-term epilepsy surgery outcomes in patients with PET-positive, MRI-negative temporal lobe epilepsy. Epilepsy Behav. 41, 91–97.

Yogarajah, M., Duncan, J.S., 2008. Diffusion-based magnetic resonance imaging and tractography in epilepsy. Epilepsia 49, 189–200.

Yoo, S.Y., Chang, K.-H., Song, I.C., Han, M.H., Kwon, B.J., Lee, S.H., Yu, I.K., Chun, C.-K., 2002. Apparent diffusion coefficient value of the hippocampus in patients with hippocampal sclerosis and in healthy volunteers. Am. J. Neuroradiol. 23, 809–812.

Zhang, J., Liu, Q., Mei, S., Zhang, X., Liu, W., Chen, H., Xia, H., Zhou, Z., Wang, X., Li, Y., 2014. Identifying the affected hemisphere with a multimodal approach in MRI-positive or negative, unilateral or bilateral temporal lobe epilepsy. Neuropsychiatr. Dis. Treat. 10, 71.